The Energetics of Electron Transfer in Redox-DNA Layers Mimics that of Redox Proteins

Zhiyong Zheng[1], Simon Grall[2], Soo Hyeon Kim[2], Arnaud Chovin[1], Nicolas Clement[2,3]*, Christophe Demaille[1]*

1 Université Paris Cité, CNRS, Laboratoire d'Electrochimie Moléculaire, F-75013 Paris, France

2 IIS, LIMMS/CNRS-IIS UMI2820, The University of Tokyo; 4-6-1 Komaba, Meguro-ku Tokyo, 153-8505, Japan

3 LAAS, 7 avenue du Colonel Roche, 31400 Toulouse, France

KEYWORDS DNA electrochemistry, low reorganization energy, Q-Biol, free energy barrier for electron transfer, Stern layer, ion solvation

ABSTRACT: Redox-DNA layers have recently demonstrated unique properties, such as reorganization energy of electron transfer that can be tuned with DNA length or hybridization, and completely suppressed under nanoconfinement. These discoveries, attributed to the changes in the solvation of the redox marker and/or fast chain dynamics, provide a unique opportunity to use electrochemical measurements as a tool to address open questions in ion solvation and to clarify the origin of low reorganization energies reported in protein electron transfer. Here, high-scan-rate, variable-temperature cyclic voltammetry, analyzed using the Marcus formalism and molecular dynamics simulations, reveals that the total free energy barrier of electron transfer consists of two additive elements: the reorganization energy of the partially desolvated redox marker and the energy cost for solvation changes of the redox marker at the solid/liquid interface. These results may have profound implications for our understanding of electron transfer and solvation effects in fast-moving molecules, providing opportunities for better design of artificial photosynthetic systems, biosensing, and energy conversion devices.

Electron transfer (ET) reactions are at the heart of the energy-generating processes of life, through photosynthesis and mitochondrial respiration. They are also ubiquitous in chemistry and central to a myriad of applications, ranging from batteries, sensors and solar cells, to hybrid quantum devices. The main parameter that determines the rate of electron transfer is its activation barrier which is largely controlled by the reorganization energy of the medium.[1–3] For electron transfer reactions between small molecules in aqueous media, reorganization energy values are typically in the range of one eV.[3]

To increase electron transfer rate and efficiency in energy transport chains, Nature minimizes reorganization energy by fine-tuning the structures of redox proteins. Energy values as low as 0.2 - 0.3 eV have been reported for electron transport proteins such as cytochrome C,[4–6] or azurin.[7,8] The exact mechanism responsible for such reorganization energy reduction is still under debate; it may notably involve the low dielectric permittivity of the hydrophobic core of proteins[4,9] or their internal fluctuation dynamics.[7,10,11]

For engineering applications, however, fine control over reorganization energy is generally lacking. The adjustments are typically restricted to modifying the solvent nature, the size, or the structure of the redox species. [12–14]

Therefore, finding new ways to significantly reduce the activation energy of electrochemical reactions would not only advance the fundamental understanding of electrochemical processes but also have far-reaching implications for the development of innovative energy conversion technologies.[13,14]

In a recent study, we shed light on an unconventional avenue to achieve this goal: we discovered that the reorganization energy of ferrocenyl (Fc) redox groups can be reduced to a few tenths of eV by attachment to DNA strands end-grafted to electrode surfaces.[15] Moreover, we showed that this effect can be further enhanced by confining the DNA in electrochemical nanogaps, ultimately leading to almost complete suppression of the reorganization energy.[16]

Specific to this system are the DNA chains moving on the nanosecond timescale, and the associated inertial and solvation effects at the solid/liquid interface.[17] Therefore, these well-controlled redox-DNA layers could be considered as ideal archetypal systems to address open questions regarding solvation mechanisms at interfaces and to understand the reduced ET reorganization energies observed for the redox proteins and enzymes that are part of the photosynthetic and respiratory energy chains. In addition, understanding these interfacial effects for redox-DNA layers could lead to optimized design rules of E-DNA- sensors, which use such layers as sensing elements.[18–24] Indeed, we have shown that modulation of the reorganization energy by the hybridization state of the DNA underlies the signaling mechanism of these sensors.[15]

Herein, we propose the first systematic study of the energetics of electron transfer in redox-DNA layers, focusing on the dependence of reorganization energy and kinetic parameters on both the driving force of ET (overpotential) and temperature. We investigate the electrochemical behavior of a series of model ferrocene – end labeled oligo-dT terminally attached to gold electrodes, using high-scan-rate cyclic voltammetry (CV), complemented by molecular dynamics simulations using the Q-Biol software we are developing. Q-Biol is based on the OxDNA package[25] and enables the complete dynamics of the anchored DNA to be numerically reproduced and resolved in time. The CV behavior of Fc-DNA is analyzed based on the Marcus-Hush-Levich-Chidsey (MHLC) electron transfer kinetic model, yielding values for the rate constant, k_o, and reorganization energy, λ, of ET. The dependence of these parameters on DNA chain length, hybridization state, and temperature is studied. We evidence that the overall free energy barrier of ET for Fc-DNA actually consists of two additive components. The first is the classical Marcus term, which depends quadratically on the electrode potential and on the reorganization energy, λ. The second component does not depend on the electrode potential, but only on the hybridization state of the DNA chain. Its dominant contribution to the total energy barrier explains the observed independence of k_o on λ. We assign this additional energy barrier for ET and the accompanying suppression of λ to the fast and inertial motion of the chain near the interface which imposes a dynamical restriction on ET and also likely promote partial desolvation of Fc.

RESULTS

Fc-DNA layers assembly and characterization

3'-ferrocene-labeled oligo $(dT)_N$ chains of various lengths (N = 10-50) were 5' thiol end-anchored into ultra-flat template-stripped gold surfaces (TS-Au), together with 6-Mercapto-1-hexanol (MCH) used as a surface diluent (see Supporting Information). The resulting diluted Fc-ssDNA layers were characterized by cyclic voltammetry (CV), in a high ionic strength electrolyte (pH 7, buffered 1 M $NaClO_4$), at various temperatures ranging from 10°C to 45°C. The surface-attached Fc-dT_N was then hybridized by exposing the electrode to fully complementary dA_N chains, and the response of the hybridized Fc-$(dT.dA)_N$ layer was characterized again by CV throughout the whole temperature range. In all cases, at slow enough scan rates, v, well-defined surface signals were recorded, such as exemplified in Figure 1a and Figure 1b, for Fc-dT_{50} and Fc-$(dT.dA)_{50}$, respectively.

The slow scan rate voltammograms exhibited all the characteristics of ideal signals resulting from a surface-limited redox species reversibly exchanging an electron at the electrode. These characteristics include peak current proportional to scan rate, peak-to-peak separation close to zero, and peak full width at half maximum close to the expected value of 3.52 F/RT.[26] Integration of the background corrected signal yielded the molar amount of Fc on the electrode, N_o. Knowing the electrode geometric surface area, S, the DNA surface coverage ensued: $\Gamma = N_o/S$. The values obtained for Γ were typically of 2 – 3 pmol/cm², corresponding to an average interchain distance, $d = 1/(N_A\Gamma)^{1/2}$ ~7-9 nm (N_A is the Avogadro constant).

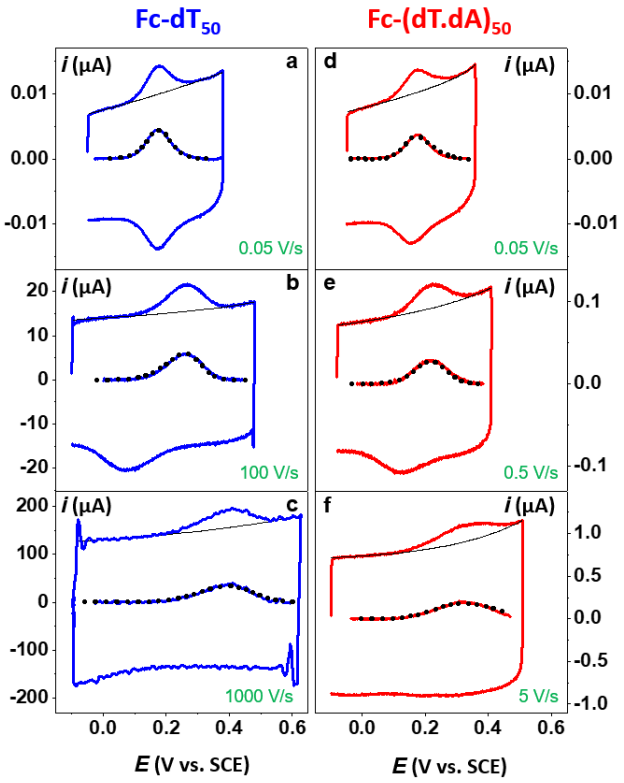

Figure 1. Cyclic voltammograms at a TS-Au electrode bearing a dilute layer of Fc-DNA chains. (a,b,c): Single stranded Fc-dT_{50}, (d,e,f) Double-stranded Fc-$(dT.dA)_{50}$. Both raw and background-corrected signals are shown. Back lines are background correction lines. Dotted curves are theoretical CVs calculated using: (a,d) Laviron's expression for ideal diffusion-less surface signals, (b,c,e,f) the MHLC model. Scan rates are indicated. Γ = 2.7 pmol/cm². Phosphate buffered, 1 M $NaClO_4$ aqueous electrolyte, pH = 7. T= 25°C.

By comparing this distance to the typical size of the end-grafted chain, either the coil size of the flexible Fc-ssDNA or the contour length of the rigid Fc-dsDNA, one reaches the conclusion that lateral interactions between neighboring chains are negligible for the two shortest DNA lengths considered here (N = 10, 20), but possibly more present for the longer ones (N = 35, 50) (See Table S1 and related discussion).

Temperature dependence of the electron transfer thermodynamics.

The first parameter characterizing the electrochemical response of the Fc-DNA layers we recorded was the standard potential, $E°$, of the DNA-bond Fc head. Its value was given by the peak potential of the slow scan rates CVs. For Fc-dT_N, $E°$ values in the range of 0.170 - 0.190 V vs. SCE were found at 25 °C, which is typical of Fc attached to DNA via an alkyl chain.[27] We observed that $E°$ values actually displayed a consistent chain length dependence, decreasing by 0.5 mV per unit increase of N (Figure S1a). This could be the consequence of the oxidation of the Fc head (Fc^+) being favored by the microenvironment prevailing inside the chain coil. This falls in line with the fact that the $E°$ for the rod-like hybridized chain was found to be practically independent of N and around ~0.165 V vs. SCE, Figure S1b.

The temperature dependence of the $E°$ of the Fc-DNA, for all the chain lengths, are presented in Figure 2a and Figure 2b, for

Fc-dT$_N$ and Fc-(dT.dA)$_N$, respectively. Note that due to its low melting temperature Fc-(dT.dA)$_{10}$ was not considered. One observed that in all cases, *E°* *decreased* linearly with *T*.

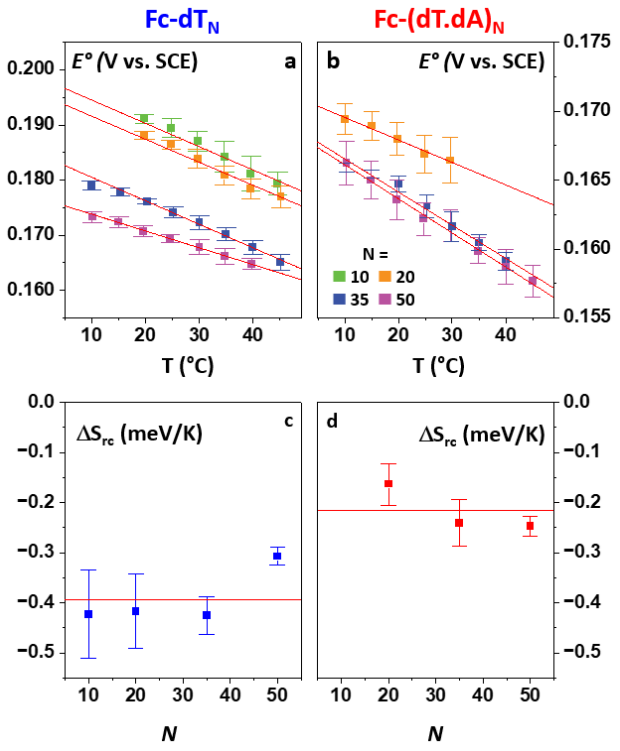

Figure 2. Temperature dependence of the electron transfer thermodynamics. Top: Temperature dependence of the standard potential of Fc-DNA chains of various length *N*, as color coded. Red lines are linear regressions of the data. Bottom: Reaction entropy ΔS_{rc}, derived from the slopes of the regression lines in (a) and (b), as a function of *N*. Horizontal lines are *N*-averaged values. (a,c) Fc-dT$_N$, (b,d) Fc-(dT.dA)$_N$.

Since these measurements were conducted in non-isothermal conditions (see Supporting Information), the slope of the *E°* vs. *T* variation was related to the reaction entropy ΔS_{rc}, i.e., the difference in absolute entropies of the reduced and oxidized form of DNA-attached Fc, by: $\Delta S_{rc} = dE°/dT$.[28,29] The ΔS_{rc} values thus derived for Fc-dT$_N$ and Fc(dT.dA)$_N$ are presented in Figures 2c and 2d, respectively. It is seen that in both cases ΔS_{rc} values are *negative* and do not markedly depend on the DNA chain length. However, the exact value of ΔS_{rc} is observed to depend on the hybridization state of the DNA chain: For Fc-ssDNA ΔS_{rc} = - 0.4 ± 0.1 meV/K, whereas for Fc-dsDNA ΔS_{rc} = - 0.2 ± 0.05 meV/K, (Mean ± SD). These values would suggest that the extent of local solvent polarization around the Fc head is sensitive to the hybridization state of the DNA chain. Electron transfer to Fc-DNA is seemingly associated with less change in entropy for dsDNA than for ssDNA.

The above ΔS_{rc} values are close to those reported for ferrocene in aqueous solution, either freely diffusing, -0.2 meV/K,[30] or surface immobilized, -0.5 meV/K.[31] For a better comparison, we also determined herein ΔS_{rc} for ferrocenedimethanol (FcdiOH), a close model of the actual DNA Fc head, in the same 1 M $NaClO_4$ aqueous electrolyte as used for Fc-DNA measurements (Figure S2). We found ΔS_{rc} = -0.60 ± 0.1 meV/K, which is close to the value measured for Fc-ssDNA. This result suggests that attachment of the Fc head to the single-stranded DNA by itself only has a minor effect on ΔS_{rc}. To the best of our knowledge, it is the first time that reaction entropies of redox-labeled DNA are measured.

Temperature dependence of the electron transfer kinetics

In order to access the kinetic parameters describing the rate of electron transfer between the electrode and the Fc head, CVs were recorded at increasingly high scan rates, reaching a few 1000 V/s. For every chain length, hybridization state and temperature considered, the CV behavior was as exemplified in Figure 1. Upon increasing the scan rate, the peak separation increased, and the peaks became broader and proportionally less intense, until they were eventually lost in the capacitive background at very high scan rates. This behavior was quantified by measuring the forward (anodic, E_{pa}) and return (cathodic, E_{pc}) peak potentials, and also the anodic peak current, i_{pa}, of CVs recorded for a wide range of scan rates. The experimental values of $E_{pa} - E°$, $E_{pc} - E°$ and of the i_{pa} / ν and $i_{pa} / \sqrt{\nu}$ normalized ratios were then plotted as a function of ν. Figure 3 shows the superimposition of two sets of such data recorded at 10°C and 45 °C, both for Fc-dT$_{50}$ (parts a,b,c) and Fc-(dT.dA)$_{50}$ (parts d,e,f).

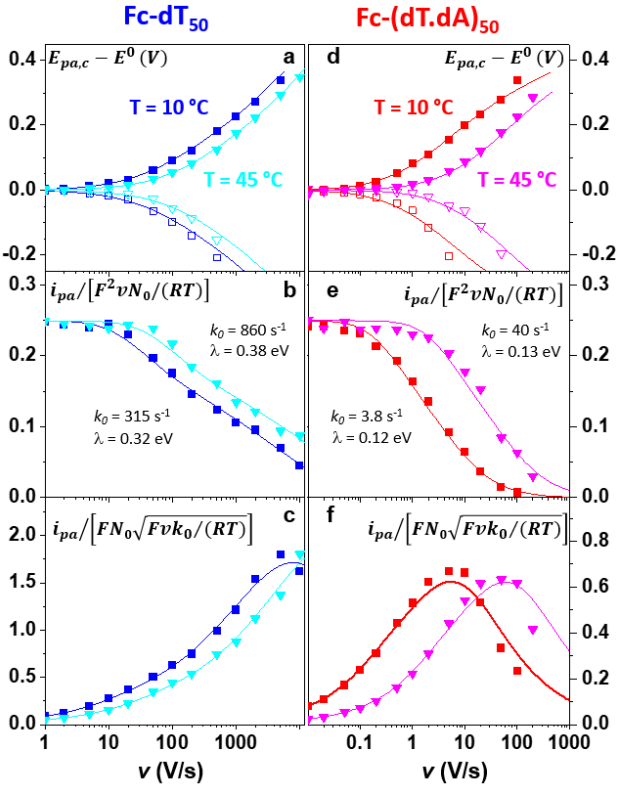

Figure 3. Dependence of the CV characteristics on scan rate, ν, at T = 10°C (cyan and pink symbols) and T = 45°C (blue and red symbols) for Fc-dT$_{50}$ (left), and Fc-(dT.dA)$_{50}$ (right). Variations of (a,d) the anodic, E_{pa}, and cathodic, E_{pc}, peak potentials, (b, e) the normalized anodic peak current i_{pa}/ν , and (c, f) $i_{pa}/\sqrt{\nu}$, ratios. Solid lines are fits to the data using the MHLC model, yielding the best-fit values of k_o and λ values indicated in (b) and (e).

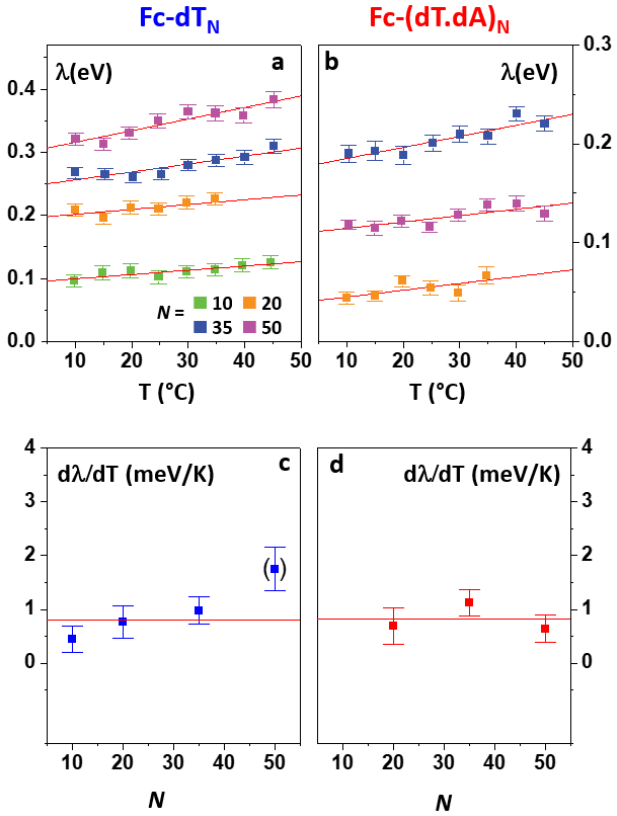

Figure 4. Analysis of the temperature-dependent reorganization energy. Top: temperature dependence of the reorganization energy, λ, for DNA chains of various lengths, *N*, as color-coded. Red lines are linear regression fits. Bottom: dependence of the temperature derivative of λ, $d\lambda/dT$, on *N*. Red lines are N-averaged values (data point in brackets excluded). (a,c) Fc-dT$_N$, (b,d) Fc-(dT.dA)$_N$.

Of particular importance is the observation that, upon increasing the scan rate, E_{pa} and E_{pc} shifted by as much as hundreds of millivolts away from $E°$, while the normalized i_{pa}/v ratio concomitantly decreased several folds. In parallel, the $i_{pa} / \sqrt{v}$ ratio tended to level off, or eventually passed through a peak value, at high enough scan rates (Figure 3f). This behavior indicates that, as the scan rate is raised, the rate of the electron transfer of the Fc head at the electrode sets the CVs characteristics.

As shown in our previous works, the DNA chain motion is infinitely fast as compared to the scan rate, as evidenced by molecular dynamics simulations of anchored DNA which revealed that the collision frequency of the Fc-head with the electrode was in the GHz range.[15,17] As a result, the CV response corresponds to that of a thin-layer cell,[26,32] which is itself formally similar to that of a diffusion-less surface-confined redox species. The electron transfer (ET) obeys Marcus-Hush-Levich-Chidsey (MHLC) kinetics.[2,33,34] This model describes the ET rate on the basis of two independent parameters: k_o, the apparent standard electron transfer rate, and λ, the reorganization energy, being four times the intrinsic activation energy of the electron transfer reaction. Theoretical CVs of a surface-attached species obeying MHLC kinetics were numerically calculated, as described previously,[15] for any set of k_o and λ values. The theoretical variation of the peak positions with scan rates depended mostly on the k_o value, and only weakly on λ.[34–36] Fitting of the E_{pa}-$E°$ and E_{pc}-$E°$ vs. v data was thus carried out using k_o as a single adjustable parameter. λ was then used as the sole fitting parameter to reproduce the i_{pa} / v vs. v dependency. Variations of the CV characteristics with scan rate were perfectly reproduced using the derived set of best-fit k_o and λ values, as exemplified in Figure 3 where solid lines are calculated curves. Importantly, the complete shape of the anodic CV wave was also well reproduced (see theoretical signals in dotted lines in Figure 1). This good agreement between theory and experiment was observed for all of the chain lengths, temperatures, and hybridization states of Fc-DNA. λ values thus obtained are plotted versus T in Figures 4a and 4b, for single-stranded and duplexed DNA, respectively.

Upon examining these plots, one can see that the absolute value of λ seems to depend on *N*, being higher for longer Fc-ssDNA chains and non-monotonously correlated to *N* for Fc-dsDNA. However, these variations are rather to be attributed to the previously identified trend of λ to linearly increase with the relative chain coverage (i.e., chain crowding).[15] What we specifically explore here is the dependence of the experimental λ values on temperature. One can observe from Figure 4a and 4b, that, for all Fc-DNA systems, λ systematically showed a small, but consistent linear *increase* with temperature. The slope of this linear variation, $d\lambda/dT$, is plotted as a function of the chain length in Figure 4c and 4d, for Fc-dT$_N$ and Fc-(dT.dA)$_N$, respectively. No clear *N* dependence of $d\lambda/dT$ was observed for either the single-stranded or duplexed chains. A common mean value of +0.8 ± 0.2 meV/K was found for this parameter.

The dependence of k_o on temperature was also carefully studied, for all DNA systems considered, Figure 5a and 5b. As previously observed,[15] k_o values were higher for the shorter chains and for single-stranded Fc-DNA.

For the sake of simplicity, we first carried out a simple Arrhenius analysis of the data, by plotting ln(k_o) vs. 1/T. This treatment assumes that k_o is related to the activation energy of the electron transfer step, E_A, by the simple expression:

$$k_o = A \exp[-E_A/RT] \qquad (1)$$

where A is a pre-exponential constant (in s^{-1}).

Hence, E_A values were obtained from the slope of the nicely linear experimental ln(k_o) vs. 1/T plot, while A values were obtained from the origin. E_A was found to be independent of the chain length, Figure 5c and 5d. Average E_A values of 0.26 ± 0.05 eV and 0.54 ± 0.05 eV were found for the single-stranded and duplexed Fc-DNA, respectively.

At this stage, one should recall that the Fc-head of the end-attached DNA strands statistically explores a few tens of nanometer radius hemispherical domain over the surface, defined by the chain length and stiffness.[15,17] The electron transfer can efficiently occur over a distance of a few angstroms away from the electrode surface. As a result, k_o is jointly modulated by the presence probability of the Fc head at the electrode (ρ_e), averaged over 10 µs in Q-biol simulations, and the integrated (heterogeneous) standard ET rate constant (k_s): $k_o = \rho_e\, k_s$. We previously showed that ρ_e displayed a marked chain length and hybridization state dependence.[15] To take this into account, one needs to consider k_s instead of k_o for

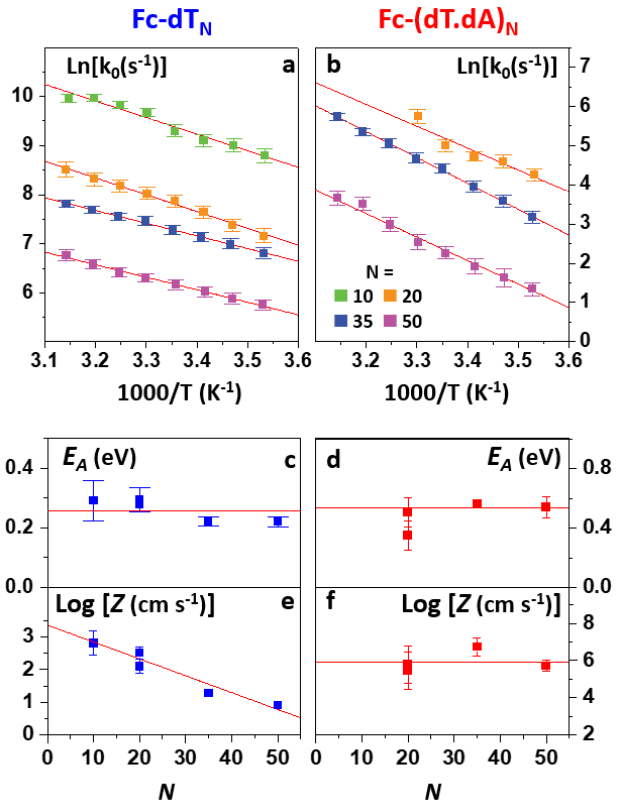

Figure 5. Arrhenius analysis of the temperature dependence of k_o for Fc-DNA. Top: ln[k_o] vs. 1/T plots for various DNA chain lengths, *N*, as color coded. Bottom: DNA chain length dependence of (c,d) the activation energy, E_A, and of (e,f) the pre-exponential factor, *Z*. (a,c,e): Fc-dT$_N$, (b,d,f): Fc-(dT.dA)$_N$. Red lines in (c,d,f) are N-averaged values and red line in (e) is a guide to the eye.

data analysis, which is to be carried out on the basis of the following equation, replacing equation (1):

$$k_s = Z \exp[-E_A/RT] \qquad (2)$$

with $Z = A/\rho_e$, a prefactor having the dimension of a heterogeneous electron transfer rate constant (cm/s).

The value of ρ_e, can be obtained for any DNA chain length, temperature, and hybridization state using the Q-Biol molecular dynamic software we developed earlier.[17] We verified that, within the temperature range we explored, ρ_e was largely temperature-independent, Figure S3. Hence *A* values were converted into Z values using the value of $\rho_e(N)$ derived from Q-Biol at 25°C.

The dependence of *Z* on chain length and hybridization state is presented in Figures 5e and 5f. *Z* is seen to decrease with increasing *N* for Fc-dT$_N$, while being *N*-independent for Fc-(dT.dA)$_N$.

DISCUSSION

Activation energies from the driving force dependence of the ET reaction

We showed here that the complete scan rate dependence of the CV response of Fc-DNA can be perfectly well reproduced by considering the MHLC model of electron transfer kinetics. This implies that the dependence of the electron transfer rate on overpotential (i.e., ET driving force) is correctly captured by the parameter λ. However, a remarkable feature, which we discovered in our previous contribution and confirmed here, is the unusually low λ values (0.05 to 0.35 eV) required to describe the response of the Fc-DNA systems, Figure 4a and 4b. This is much smaller than the reorganization energy value of ~0.85 eV usually reported for ferrocene in solution or immobilized on surfaces via rigid alkyl thiol chains.[33,37–39] It is important to note that in the latter case, reorganization energies were preferably determined from the temperature dependence of k_o on *T* rather than by analysis of the CV response.

The reason was that the CVs of such layers often displayed non-ideal characteristics, even at slow scan rates, being broader than predicted by Laviron's model.[38,40] Similarly, non-ideal, i.e., non-monoexponential, chronoamperograms were frequently reported.[38,41,42] This was regarded as resulting from a dispersion in standard potentials and/or electron transfer rate constants in the Fc population.[38,42–44] It was thus concluded that, because of such artifacts, CV analysis was unsuitable and potentially led to underestimated λ values.

However, we emphasize that, for Fc-DNA layers, the slow scan rate signals we recorded could be perfectly fitted with Laviron's model, corresponding to a *single population* of non-interacting ferrocene heads located outside the double layer and undergoing rapid electron transfer (dotted signals in Figure 1a and 1b). Besides, as a control, we also recorded chronoamperograms at Fc-DNA layers, and they displayed the single mono-exponential decay expected for a single, kinetically well-defined, Fc population, Figure S4. These two last results rule out thermodynamic or kinetic dispersion as the reason for the low λ values derived here. We thus claim that low reorganization energies do correspond to an intrinsic property of Fc-DNA.

The fact that the CV behavior of Fc-DNA could be well described by the MHLC model implies that the overall activation energy of the electron transfer ($\Delta G^{\ddagger}$) contains a contribution of $\Delta G_E^{\ddagger}$, which displays the classical quadratic dependence on the driving force of the reaction, -*F* (*E*-*E*°):[45]

$$\Delta G_E^{\ddagger} = \Delta G_0^{\ddagger}\left[1 - F(E - E°)/\left(4\Delta G_0^{\ddagger}\right)\right]^2$$

With $\Delta G_0^{\ddagger}$ the intrinsic free energy of activation (the intrinsic barrier, i.e., $\Delta G_E^{\ddagger}$ for $E = E°$), which is related to λ by: $\Delta G_0^{\ddagger} = \lambda/4$. Classically λ equals the sum of the internal bonds and solvent reorganization energies.

The intrinsic barrier can be decomposed into its enthalpic, ($\Delta H_0^{\ddagger}$) and entropic ($\Delta S_0^{\ddagger}$) components as:

$$\Delta G_0^{\ddagger} = \Delta H_0^{\ddagger} - T\Delta S_0^{\ddagger} \qquad (3)$$

As a result, the slope of the experimental λ vs. *T* variations (Figure 4a and 4b), is: $d\lambda/dT = -4\,\Delta S_0^{\ddagger}$. The positive $d\lambda/dT$ values obtained for all chain lengths and hybridization states thus first show that $\Delta S_0^{\ddagger}$ is *negative*. More quantitatively $d\lambda/dT$ plots yielded $\Delta S_0^{\ddagger}$ = -0.2 ± 0.05 meV/K for both Fc-dT$_N$ and Fc-(dT.dA)$_N$.

For a species such as Fc, which a priori exhibits a symmetrical ET energy barrier, a coarse estimate for the activation entropy can be obtained from the value of the reaction entropy, ΔS_{rc}, by :[46–48] $\Delta S_0^{\ddagger} = 0.5\,\Delta S_{rc}$

From the here-determined ΔS_{rc} values, $\Delta S_0^{\ddagger}$ is thus predicted to be in the order of around -0.20 meV/K and -0.1 meV/K for Fc-ssDNA and Fc-dsDNA respectively.

The relatively good quantitative agreement between these predictions and the measured $\Delta S_0^{\ddagger}$ values indicate that the activation energies measured here, and hence the λ values, do describe the energetics of the electron transfer reaction of Fc-DNA at the electrode. Importantly, we note that a similar activation entropy value of -0.1 meV/K was reported for the electron transfer reaction in self-assembled alkyl ferrocene layers.[47]

Because of the necessarily limited temperature range explored, $\Delta H_0^{\ddagger}$ values could not be reliably obtained from the extrapolation of $d\lambda/dT$ plot to zero Kelvin. Plotting λ/T vs. $1/T$ was found to be equally error-prone. However, $\Delta H_0^{\ddagger}$ could be estimated from equation (3), applied at T = 25°C, using the λ values determined for this temperature. This led to very small $\Delta H_0^{\ddagger}$ values, in the order of a fraction of meV, for all chain lengths and hybridization states. By contrast, for alkyl-Fc layers, a much larger $\Delta H_0^{\ddagger}$ value of ~0.2 eV has been reported.[47] Hence, it seems safe to consider that, for Fc-DNA, at accessible temperatures, $\Delta G_0^{\ddagger} \sim -T\Delta S_0^{\ddagger}$, i.e., the entropic barrier determines the value of λ.

We can finally conclude that the origin of the particularly lower λ values measured for DNA than for alky-Fc layers lies in the enthalpic component of the activation energy, being almost entirely suppressed in the case of Fc-DNA. On the opposite, the activation entropy for Fc-DNA remains the same as for Fc-alkyl layers.

Activation energy from the temperature dependence of the ET reaction rate

The above Arrhenius analysis assumed that k_s was related to the activation energy via equation (2). Yet, a more general expression would be:

$k_s = Z' \exp[-\Delta G_0^{\ddagger}/RT]$ with Z' as a pre-exponential term discussed below.

As a result, from Equation (3), it is clear that E_A is expected to be the intrinsic *enthalpy* of the reaction, i.e., $\Delta H_0^{\ddagger}$.

However, the E_A values derived from the Arrhenius analysis, ~ 0.26 eV for Fc-ssDNA and 0.54 eV for Fc-dsDNA, are much larger than the vanishingly low $\Delta H_0^{\ddagger}$ values estimated above from λ (and even larger than λ/4 altogether). These seemingly conflicting results suggest that the activation energy for Fc-DNA is much larger than what could be expected from λ (and for Fc-dsDNA is even twice as large as one-fourth of λ for free Fc). One thus needs to define a larger, *overall*, activation energy of electron transfer, $\Delta G_T^{\ddagger}$, which contains two unrelated components: the driving force-dependent term, $\Delta G_E^{\ddagger}$, and a driving force-independent term, $\Delta G_{DNA}^{\ddagger}$:

$$\Delta G_T^{\ddagger} = \Delta G_E^{\ddagger} + \Delta G_{DNA}^{\ddagger}$$

so that a general expression for the electron transfer rate at a potential E is:

$$k(E) = Z' \exp[-\Delta G_E^{\ddagger}/RT] \exp[-\Delta G_{DNA}^{\ddagger}/RT]$$

thus:

$$k_s = Z' \exp[-\Delta G_0^{\ddagger}/RT] \exp[-\Delta G_{DNA}^{\ddagger}/RT]$$

$$= Z' \exp[-\lambda/(4RT)] \exp[-\Delta G_{DNA}^{\ddagger}/RT] \quad (4)$$

As a result, the CV analysis of the driving force dependence of ET kinetics yielded the value of $\lambda = 4\,\Delta G_0^{\ddagger}$, while the Arrhenius analysis yielded $E_A = \Delta H_0^{\ddagger} + \Delta H_{DNA}^{\ddagger}$.

Since, as seen above, $\Delta H_0^{\ddagger}$ is around zero, while the values found for E_A are rather large and in the range of 0.26 – 0.54 eV, we conclude that $E_A \sim \Delta H_{DNA}^{\ddagger}$.

Overall, the total intrinsic free energy of activation is:

$$\Delta G_{T,0}^{\ddagger} = \Delta G_0^{\ddagger} + \Delta G_{DNA}^{\ddagger} = \lambda/4 + \Delta G_{DNA}^{\ddagger}$$

$$= \lambda/4 + \Delta H_{DNA}^{\ddagger} - T\Delta S_{DNA}^{\ddagger}$$

Hence, it appears that the rate of electron transfer to Fc-DNA is jointly controlled by the kinetics of the electron transfer step itself, featuring a small λ value, and by a second thermally activated process. This process is characterized by a relatively large activation enthalpy, in the order of ~0.26 eV for Fc-ssDNA and 0.54 eV for the duplex. Assaying its entropic component requires that the value of the prefactor, Z, is examined and discussed.

Analysis of the pre-exponential factor Z

Equation (4) can be written as follows, in order to detail the entropic contributions to k_s:

$$k_s = Z' \exp[-\Delta G_0^{\ddagger}/RT] \times \exp[-\Delta G_{DNA}^{\ddagger}/RT]$$

$$= Z' \exp[-(\Delta H_0^{\ddagger} - T\Delta S_0^{\ddagger})/RT] \times \exp[-(\Delta H_{DNA}^{\ddagger} - T\Delta S_{DNA}^{\ddagger})/RT]$$

Since $\Delta H_0^{\ddagger}$ is negligible compared to $T\Delta S_0^{\ddagger}$:

$$k_s = Z' \exp[(\Delta S_0^{\ddagger} + \Delta S_{DNA}^{\ddagger})/R] \times \exp[-(\Delta H_{DNA}^{\ddagger})/RT]$$

Hence, the origin of the Arrhenius plot actually yielded the value of:

$$Z = Z' \exp[(\Delta S_0^{\ddagger} + \Delta S_{DNA}^{\ddagger})/R]$$

Consequently, the value of $\Delta S_{DNA}^{\ddagger}$ can be obtained from the experimental Z value (Figure 5), provided Z' is known.

The MHLC model, refined by Feldberg and Sutin,[49] predicts the following equation for the integrated standard heterogeneous electron transfer rate constant k_s, in the case a non-adiabatic electron transfer :

$$k_s = Z' exp\left[-\frac{\lambda^*}{4}\right] \quad (5)$$

$$\text{where } Z' = \frac{2\pi^2 \rho {H_0}^2}{\beta h \sqrt{1+\lambda^*/\pi}} \quad (6)$$

with $\lambda^* = \lambda/RT$, ρ is the density of states in the metal electrode, β the tunneling decay constant (~1 Å^{-1}), H_o the electronic coupling term (at the closest approach distance from the electrode), h the Planck constant.

Non-adiabaticity of the electron transfer is guaranteed here by the presence of the MCH layer, which ensures weak electronic coupling between the Fc head and the electrode.

Note that Z' displays a temperature dependence through the $\sqrt{1+\lambda^*/\pi}$ term at the denominator. However, within the narrow range of temperature explored, and due to the low λ values found, this term remained approximately constant here. This legitimates the use of the simple Arrhenius equation (2) for data analysis.

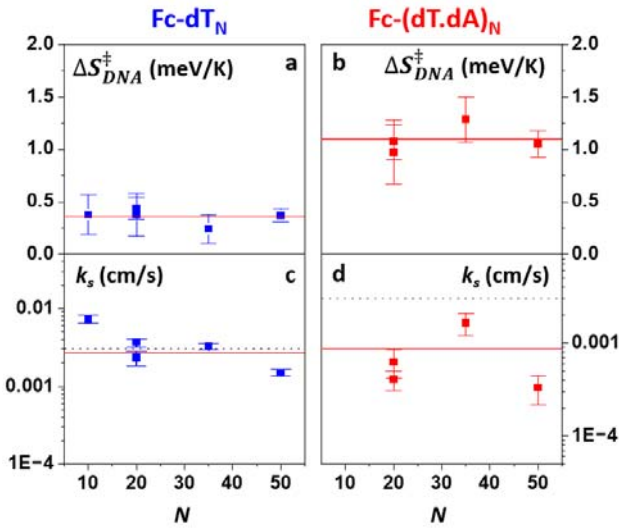

Figure 6. Chain length (*N*) dependence of (a,b) the DNA-specific entropic term, $\Delta S^{\ddagger}_{DNA}$, and (c,d) the standard heterogeneous electron transfer rate constant, k_s (at 25°C). (a,c): Fc-dT$_N$, (b,d): Fc-(dT.dA)$_N$. The red lines are N-averaged values. The dotted lines in (c) and (d) represent the k_s value for FcdiOH at an MCH-coated TS-Au electrode in 1 M $NaClO_4$.

Applying equation (5) to the case of the model compound FcdiOH, for which the values of k_s and λ were previously measured,[15] enables the term $\frac{2\pi^2 \rho {H_0}^2}{\beta h}$ appearing in equation (6) to be evaluated. This, in turn, allows *Z'* values for Fc-DNA to be estimated, see supporting information.

Knowing the values of *Z*, *Z'* and $\Delta S^{\ddagger}_0$ for Fc-DNA enables $\Delta S^{\ddagger}_{DNA}$ to be derived for any chain length and hybridization state from:

$$\Delta S^{\ddagger}_{DNA} = \mathrm{R}\ln(Z/Z') - \Delta S^{\ddagger}_0$$

Figures 6a and 6b show $\Delta S^{\ddagger}_{DNA}$ values thus calculated, for all chain lengths and hybridization state. $\Delta S^{\ddagger}_{DNA}$ is found to be independent of *N*, but to depend on the hybridization state of the chain, having values of ~ +0.36 ± 0.05 meV/K and ~ +1.1 ± 0.2 meV/K for the single-stranded and duplexed Fc-DNA, respectively.

One can finally estimate the value of the driving-force independent free activation energy, $\Delta G^{\ddagger}_{\mathrm{DNA}} = \Delta H^{\ddagger}_{\mathrm{DNA}} - T\Delta S^{\ddagger}_{\mathrm{DNA}}$, which is found to be worth 0.17 eV and 0.24 eV at T = 25°C, for Fc-ssDNA and Fc-dsDNA, respectively. Note that $G^{\ddagger}_{\mathrm{DNA}}$ is only slightly higher for Fc-dsDNA than for Fc-ssDNA, despite a ~ 2 times larger $\Delta H^{\ddagger}_{\mathrm{DNA}}$ value for the duplex than for the single-stranded chain. This is due to mutual compensation between the enthalpic and entropic terms, since $\Delta S^{\ddagger}_{\mathrm{DNA}}$ is also larger for Fc-dsDNA than for Fc-ssDNA.

Importantly, $\Delta G^{\ddagger}_{\mathrm{DNA}}$ is found to be in any case much greater than $\Delta G^{\ddagger}_0 = \lambda/4$, whose value was in the range of 0.025 – 0.1 eV for Fc-ssDNA and 0.0125- 0.05 eV for Fc-dsDNA (Figure 4), Hence, at $E = E°$, the overall intrinsic activation energy for Fc-DNA, $\Delta G^{\ddagger}_{T,0} = \Delta G^{\ddagger}_0 + \Delta G^{\ddagger}_{DNA} = \lambda/4 + \Delta G^{\ddagger}_{DNA}$, is largely set by the driving-force independent barrier, $\Delta G^{\ddagger}_{\mathrm{DNA}}$.

The standard heterogeneous ET rate constant of Fc-DNA

To determine the influence of the different components of the activation energy for Fc-DNA on the absolute value of k_s (at T=25°C), we compared the k_s values we obtained for Fc-DNA ($k_s = k_o/\rho_e$) with those we determined for FcdiOH, Figures 6c and 6d. For Fc-ssDNA, k_s was found to be around ~7 × 10^{-3} cm/s for N = 10 and ~ 3 × 10^{-3} cm/s for higher N values. For Fc-dsDNA, the k_s values were scattered in the 0.6-1.8 × 10^{-3} cm/s range.

The first striking result is that k_s values for Fc-DNA and for FcdiOH are coarsely of the same order of magnitude. This result, we also obtained previously,[15] seemed paradoxical, considering that λ values for Fc-DNA were much smaller than that characteristic of ferrocene species. Indeed, the exponential dependence of the electron transfer rates on λ should have resulted in k_s being orders of magnitude *faster* for Fc-DNA's. The present study enables us to understand the reason behind this paradox: the contribution of an extra thermally activated process to the ET thermodynamics, which increases the activation energy by $\Delta G^{\ddagger}_{DNA}$ and consequently decreases the k_s value. Besides, the fact that $\Delta G^{\ddagger}_{DNA}$ is much larger than the λ values found for Fc-DNA renders the k_s value almost independent of λ. Additionally, the larger $\Delta G^{\ddagger}_{\mathrm{DNA}}$ value for the duplex than for the single-strand justifies the lower k_s value for Fc-dsDNA compared to Fc-ssDNA.

Origin of the extra free energy barrier and of the low λ values for Fc-DNA

We note that the existence of a component of the overall activation free energy, which does not depend on the electrochemical driving force (-F(E-E°)), is taken into account in the full formulation of Marcus equation:[2]

$$\Delta G^{\ddagger}_{E} = w_r + \frac{\lambda}{4}\left(1 - [F(E - E°) + w_p - w_r]/\lambda\right)^2 \qquad (7)$$

This component, termed w_r, is defined as the work to bring the reactants to the ET distance. w_p is the equivalent term for the products. These work terms can have an electrostatic origin, and in that case, they represent the energy cost for a (charged) redox species to approach the outer Helmholtz plane, where electron transfer is expected to occur. The highly charged nature of the DNA chain may suggest that such kind of electrostatic effects could be at play here.[50] However, the ionic strength of the electrolyte used here (1 M) is high enough for the interactions between the DNA and the electrode to be effectively shielded.[51] Besides, this scenario cannot justify the low λ values we obtained for Fc-DNA. Equation (7) with $w_r = \Delta G^{\ddagger}_{\mathrm{DNA}}$ and $w_p - w_r = 0$ can still account for our results, provided it is complemented by a mechanism that justifies a reduction of λ.

Solvation effects at the solid/liquid interface come naturally to mind as such a mechanism, for the following reasons. Firstly, in this scenario, the Fc would undergo partial desolvation near the interface, as reported for solvated ions near solid interfaces,[52–54] and this process would then be characterized by an extra contribution to the overall energy barrier. Secondly, electron transfer between the partially desolvated Fc and the electrode would then obviously be associated with a

low solvent reorganization energy (which for Fc is the dominant component of the overall reorganization energy).[55] Desolvation would thus act as a pre-equilibrium to the electron transfer step itself, reducing its overall rate. Admittedly, modulation of the activation energy by partial desolvation of the ferrocene moiety has not been observed for ferrocene derivatives in solution, nor for those attached to rigid alkylthiol layers. Therefore, we can only assume that a specific factor, unique to Fc attached to the surface via a flexible chain, is at play here and makes desolvation effects perceptible. Such a factor could be the spring-like or inertial behavior of the chain,[17] which could provide enough energy for Fc to penetrate deeper into the Stern layer where lowered reorganization energies are expected.[56] This phenomenon is expected to be stronger for Fc-dsDNA than for Fc-ssDNA, which is consistent with the lower λ values we typically obtain for the duplex.

Another possibility is that the nanosecond timescale related to the tethered DNA motion plays a role in the lowering of λ. It is known that the dielectric constant of water follows a Debye distribution whose value drops above 15 GHz, an effect that could be extended to lower frequencies near interfaces.[57]

Finally, as has been proposed by Matsyushov et al., to explain the low λ values measured for redox proteins, chain dynamics (i.e., relaxation time), in addition to the Gibbs energy, could be modulating the electron transfer activation barrier.[58,59] Specifically, some parts of the configurational space of the system could be unreachable due to dynamical restrictions, leading to a non-ergodic sampling. It is for example clear that accessible configurations may be restricted for the Fc (and its molecular orbitals) when facing the surface, due to its attachment to DNA. Regarding the characteristic time constants, most chain configurations are reached on the microsecond timescale, while the time frame for the electron transfer is in the nanosecond time range, corresponding to the Fc/electrode collision frequency. Desolvation of the Fc at the electrode would amplify such an effect.

CONCLUSION

We reveal that the free energy barrier for the electron transfer of Fc-DNA contains both a driving force-dependent component, characterized by reorganization energy λ, and a driving force-independent component, term $\Delta \boldsymbol{G}^{\ddagger}_{\boldsymbol{DNA}}$. We confirm here that λ values for Fc-DNA are greatly reduced as compared to free ferrocene and can be as low as a few tens of meVs. We provide new insights in showing that such a reduction is actually due to an almost complete suppression of the *enthalpic* component of λ for Fc-DNA while its *entropic* component remains largely unchanged. On the opposite, we have evidenced that $\Delta \boldsymbol{G}^{\ddagger}_{\boldsymbol{DNA}}$ is fairly large, in the order of 0.2 eV at 25 °C, so that it dominates the overall activation energy for electron transfer of Fc-DNA. This makes the standard heterogeneous rate constant for electron transfer, k_s, almost λ independent and explains why k_s for Fc-DNA is not as high as could be expected from the low λ values typical of Fc-DNA. Incidentally, k_s for Fc-DNA is actually comparable to that typical of free Fc, because $\Delta \boldsymbol{G}^{\ddagger}_{\boldsymbol{DNA}}$ is the same order of magnitude as the intrinsic free energy barrier typical of Fc (~1/4 × 0.85 eV). We attribute the additional energy barrier, $\Delta \boldsymbol{G}^{\ddagger}_{\boldsymbol{DNA}}$, and the lowering of λ to both the desolvation of Fc at the interface, induced by the inertial motion of the DNA, and the non-ergodic sampling of the configuration space of the system. Our findings also reveal the similarity between electron transfer in redox DNA layers and in redox protein layers, both exhibiting low reorganization energies associated to internal dynamic fluctuations. DNA layers may thus prove to be ideal model systems for understanding the dynamical effects in biological energy transfer processes.

MATERIALS AND METHODS

See Supporting Information.

ASSOCIATED CONTENT

Supporting information Materials and methods. Assaying the occurrence of lateral chain-chain interactions in Fc-DNA layers. Variation of the standard potential of Fc-DNA vs. N and of ferrocenedimethanol vs. T. Extra Q-Biol simulation data: Temperature and chain length dependence of ρ_e. Chronoamperogram of Fc-DNA.

Corresponding Authors

Dr. Christophe Demaille - Université Paris Cité, CNRS, Laboratoire d'Electrochimie Moléculaire, F-75013 Paris, France. E-mail: Christophe.demaille@u-paris.fr.
Dr. Nicolas Clément - IIS, LIMMS/CNRS-IIS UMI2820, The University of Tokyo; 4-6-1 Komaba, Meguro-ku Tokyo, 153-8505, Japan. E-mail: nclement@iis.u-tokyo.ac.jp.
LAAS, 7 avenue du Colonel Roche, 31400 Toulouse, France nclement@laas.fr

Author Contributions

C. Demaille and N. Clément obtained the funding, supervised the project and designed the experiments. Z. Zheng conducted the CV characterizations and analyzed the results. A. Chovin designed the setup and discussed the results. C.S.H. Kim provided scientific interactions on DNA electrochemistry and related simulations. S. Grall conducted Q-Biol simulations. C. Demaille, N. Clément and Z. Zheng co-wrote the paper with scientific interpretation and comments from all authors.

Notes

The authors declare no competing financial interests.

ACKNOWLEDGMENT

This work has received financial support from the French "Agence Nationale de la Recherche" (ANR), through the "SIBI" project (ANR- 19-CE42-0011-01), and from the Unicorn-Dx EU-Attract project.

REFERENCES

(1) Marcus, R. A. On the Theory of Oxidation-Reduction Reactions Involving Electron Transfer. I. *J. Chem. Phys.* **1956**, *24* (5), 966–978. https://doi.org/10.1063/1.1742723.
(2) Marcus, R. A. On the Theory of Electron-Transfer Reactions. VI. Unified Treatment for Homogeneous and Electrode Reactions. *J. Chem. Phys.* **1965**, *43* (2), 679–701. https://doi.org/10.1063/1.1696792.
(3) Piechota, E. J.; Meyer, G. J. Introduction to Electron Transfer: Theoretical Foundations and Pedagogical Examples. *J.*

Chem. Educ. **2019**, *96* (11), 2450–2466. https://doi.org/10.1021/acs.jchemed.9b00489.

(4) Jasaitis, A.; Rappaport, F.; Pilet, E.; Liebl, U.; Vos, M. H. Activationless Electron Transfer through the Hydrophobic Core of Cytochrome c Oxidase. *Proc. Natl. Acad. Sci. U. S. A.* **2005**, *102* (31), 10882–10886. https://doi.org/10.1073/pnas.0503001102.

(5) Alvarez-Paggi, D.; Castro, M. A.; Tórtora, V.; Castro, L.; Radi, R.; Murgida, D. H. Electrostatically Driven Second-Sphere Ligand Switch between High and Low Reorganization Energy Forms of Native Cytochrome C. *J. Am. Chem. Soc.* **2013**, *135* (11), 4389–4397. https://doi.org/10.1021/ja311786b.

(6) Seyedi, S. S.; Waskasi, M. M.; Matyushov, D. V. Theory and Electrochemistry of Cytochrome C. *J. Phys. Chem. B* **2017**, *121* (19), 4958–4967. https://doi.org/10.1021/acs.jpcb.7b00917.

(7) Sarhangi, S. M.; Matyushov, D. V. Anomalously Small Reorganization Energy of the Half Redox Reaction of Azurin. *J. Phys. Chem. B* **2022**, *126* (16), 3000–3011. https://doi.org/10.1021/acs.jpcb.2c00338.

(8) Khoshtariya, D. E.; Dolidze, T. D.; Shushanyan, M.; Davis, K. L.; Waldeck, D. H.; van Eldik, R. Fundamental Signatures of Short- and Long-Range Electron Transfer for the Blue Copper Protein Azurin at Au/SAM Junctions. *Proc. Natl. Acad. Sci. U. S. A.* **2010**, *107* (7), 2757–2762. https://doi.org/10.1073/pnas.0910837107.

(9) Krishtalik, L. I. The Medium Reorganization Energy for the Charge Transfer Reactions in Proteins. *Biochim. Biophys. Acta - Bioenerg.* **2011**, *1807* (11), 1444–1456. https://doi.org/https://doi.org/10.1016/j.bbabio.2011.07.002.

(10) Matyushov, D. V. Protein Electron Transfer: Dynamics and Statistics. *J. Chem. Phys.* **2013**, *139* (2), 25102. https://doi.org/10.1063/1.48127788.

(11) Matyushov, D. V. Reorganization Energy of Electron Transfer. *Phys. Chem. Chem. Phys.* **2023**, *25* (11), 7589–7610. https://doi.org/10.1039/D2CP06072H.

(12) Zimmt, M. B.; Waldeck, D. H. Exposing Solvent's Roles in Electron Transfer Reactions: Tunneling Pathway and Solvation. *J. Phys. Chem. A* **2003**, *107* (19), 3580–3597. https://doi.org/10.1021/jp022213b.

(13) Shi, Y.; Chang, Y.; Lu, K.; Chen, Z.; Zhang, J.; Yan, Y.; Qiu, D.; Liu, Y.; Adil, M. A.; Ma, W.; Hao, X.; Zhu, L.; Wei, Z. Small Reorganization Energy Acceptors Enable Low Energy Losses in Non-Fullerene Organic Solar Cells. *Nat. Commun.* **2022**, *13* (1), 3256. https://doi.org/10.1038/s41467-022-30927-y.

(14) Fort, M. J.; Click, S. M.; Robinson, E. H.; He, F. M. C.; Bernhardt, P. V; Rosenthal, S. J.; Macdonald, J. E. Minimizing the Reorganization Energy of Cobalt Redox Mediators Maximizes Charge Transfer Rates from Quantum Dots. *Angew. Chemie Int. Ed.* **2022**, *61* (27), e202202322. https://doi.org/https://doi.org/10.1002/anie.202202322.

(15) Zheng, Z.; Kim, S. H.; Chovin, A.; Clement, N.; Demaille, C. Electrochemical Response of Surface-Attached Redox DNA Governed by Low Activation Energy Electron Transfer Kinetics. *Chem. Sci.* **2023**, *14* (13), 3652–3660. https://doi.org/10.1039/d3sc00320e.

(16) Zheng, Z.; Grall, S.; Kim, S. H.; Chovin, A.; Clement, N.; Demaille, C. Activationless Electron Transfer of Redox-DNA in Electrochemical Nanogaps. *J. Am. Chem. Soc.* **2024**, *146* (9), 6094–6103. https://doi.org/10.1021/jacs.3c13532.

(17) Madrid, I.; Zheng, Z.; Gerbelot, C.; Fujiwara, A.; Li, S.; Grall, S.; Nishiguchi, K.; Kim, S.-H.; Chovin, A.; Demaille, C.; Clement, N. Ballistic Brownian Motion of Nanoconfined DNA. *ACS Nano* **2023**, *17* (17), 17031–17040. https://doi.org/10.1021/acsnano.3c04349.

(18) Lubin, A. A.; Plaxco, K. W. Folding-Based Electrochemical Biosensors: The Case for Responsive Nucleic Acid Architectures. *Acc. Chem. Res.* **2010**, *43* (4), 496–505. https://doi.org/10.1021/ar900165x.

(19) Du, Y.; Dong, S. Nucleic Acid Biosensors: Recent Advances and Perspectives. *Anal. Chem.* **2017**, *89* (1), 189–215. https://doi.org/10.1021/acs.analchem.6b04190.

(20) Ferapontova, E. E. DNA Electrochemistry and Electrochemical Sensors for Nucleic Acids. *Annu. Rev. Anal. Chem.* **2018**, *11* (1), 197–218. https://doi.org/10.1146/annurev-anchem-061417-125811.

(21) Ranallo, S.; Porchetta, A.; Ricci, F. DNA-Based Scaffolds for Sensing Applications. *Anal. Chem.* **2019**, *91* (1), 44–59. https://doi.org/10.1021/acs.analchem.8b05009.

(22) Pellitero, M. A.; Shaver, A.; Arroyo-Currás, N. Critical Review—Approaches for the Electrochemical Interrogation of DNA-Based Sensors: A Critical Review. *J. Electrochem. Soc.* **2019**, *167* (3), 37529. https://doi.org/10.1149/2.0292003jes.

(23) Dauphin-Ducharme, P.; Ploense, K. L.; Arroyo-Curras, N.; Kippin, T. E.; Plaxco, K. W. Electrochemical Aptamer-Based Sensors. In *A Platform Approach to High-Frequency Molecular Monitoring In Situ in the Living Body*; Methods in Molecular Biology; Humana Press Inc., 2022; pp 479-492 BT-Methods in Molecular Biology. https://doi.org/10.1007/978-1-0716-1803-5_25.

(24) Gupta, V.; Dick, J. E. Real-Time Intracellular Analysis of Kanamycin Using Microaptasensors. *ACS Sensors* **2023**, *8* (3), 1143–1150. https://doi.org/10.1021/acssensors.2c02427.

(25) Snodin, B. E. K.; Randisi, F.; Mosayebi, M.; Šulc, P.; Schreck, J. S.; Romano, F.; Ouldridge, T. E.; Tsukanov, R.; Nir, E.; Louis, A. A.; Doye, J. P. K. Introducing Improved Structural Properties and Salt Dependence into a Coarse-Grained Model of DNA. *J. Chem. Phys.* **2015**, *142* (23), 234901. https://doi.org/10.1063/1.4921957.

(26) Laviron, E. General Expression of the Linear Potential Sweep Voltammogram in the Case of Diffusionless Electrochemical Systems. *J. Electroanal. Chem.* **1979**, *101*, 19–28. https://doi.org/10.1016/S0022-0728(79)80075-3.

(27) Ge, D.; Levicky, R. A Comparison of Five Bioconjugatable Ferrocenes for Labeling of Biomolecules. *Chem. Commun.* **2010**, *46* (38), 7190–7192. https://doi.org/10.1039/CoCC02044C.

(28) Yee, E. L.; Cave, R. J.; Guyer, K. L.; Tyma, P. D.; Weaver, M. J. A Survey of Ligand Effects upon the Reaction Entropies of Some Transition Metal Redox Couples. *J. Am. Chem. Soc.* **1979**, *101* (5), 1131–1137. https://doi.org/10.1021/ja00499a013.

(29) Taniguchi, V. T.; Sailasuta-Scott, N.; Anson, F. C.; Gray, H. B. Thermodynamics of Metalloprotein Electron Transfer Reactions. **1980**, 52 (10), 2275–2281. https://doi.org/doi:10.1351/pac198052102275.

(30) Sahami, S.; Weaver, M. J. Deficiencies of the Ferricinium-Ferrocene Redox Couple for Estimating Transfer Energies of Single Ions. *J. Solution Chem.* **1981**, *10* (3), 199–208. https://doi.org/10.1007/BF00653097.

(31) Hupp, J. T.; Weaver, M. J. Utility of Surface Reaction Entropies for Examining Reactant-Solvent Interactions at Electrochemical Interfaces. Ferricinium-Ferrocene Attached to Platinum Electrodes. *J. Electrochem. Soc.* **1984**, *131* (3), 619. https://doi.org/10.1149/1.2115639.

(32) Hubbard, T.; Anson, F. C. The Theory and Practice of Electrochemistry with Thin Layer Cells. In *Electroanalytical Chemistry: A Series of Advances*; 1970; pp 129–214.

(33) Chidsey, C. E. D. Free Energy and Temperature Dependence of Electron Transfer at the Metal-Electrolyte Interface. *Science (80-.).* **1991**, *4996* (251), 919–922. https://doi.org/10.1126/science.251.4996.919.

(34) Savéant, J.-M. Effect of the Electrode Continuum of States in Adiabatic and Nonadiabatic Outer-Sphere and Dissociative Electron Transfers. Use of Cyclic Voltammetry for Investigating Nonlinear Activation-Driving Force Laws. *J. Phys. Chem. B* **2002**, *106* (36), 9387–9395. https://doi.org/10.1021/jp0258006.

(35) Weber, K.; Creager, S. E. Voltammetry of Redox-Active

Groups Irreversibly Adsorbed onto Electrodes. Treatment Using the Marcus Relation between Rate and Overpotential. *Anal. Chem.* **1994**, *66* (19), 3164–3172. https://doi.org/10.1021/ac00091a027.

(36) Nahir, T. M.; Clark, R. A.; Bowden, E. F. Linear-Sweep Voltammetry of Irreversible Electron Transfer in Surface-Confined Species Using the Marcus Theory. *Anal. Chem.* **1994**, *66* (15), 2595–2598. https://doi.org/10.1021/ac00087a027.

(37) Smalley, J. F.; Feldberg, S. W.; Chidsey, C. E. D.; Linford, M. R.; Newton, M. D.; Liu, Y.-P. The Kinetics of Electron Transfer Through Ferrocene-Terminated Alkanethiol Monolayers on Gold. *J. Phys. Chem.* **1995**, *99* (35), 13141–13149. https://doi.org/10.1021/j100035a016.

(38) Richardson, J. N.; Peck, S. R.; Curtin, L. S.; Tender, L. M.; Terrill, R. H.; Carter, M. T.; Murray, R. W.; Rowe, G. K.; Creager, S. E. Electron-Transfer Kinetics of Self-Assembled Ferrocene Octanethiol Monolayers on Gold and Silver Electrodes from 115 to 170 K. *J. Phys. Chem.* **1995**, *99* (2), 766–772. https://doi.org/10.1021/j100002a046.

(39) Smalley, J. F.; Finklea, H. O.; Chidsey, C. E. D.; Linford, M. R.; Creager, S. E.; Ferraris, J. P.; Chalfant, K.; Zawodzinsk, T.; Feldberg, S. W.; Newton, M. D. Heterogeneous Electron-Transfer Kinetics for Ruthenium and Ferrocene Redox Moieties through Alkanethiol Monolayers on Gold. *J. Am. Chem. Soc.* **2003**, *125* (7), 2004–2013. https://doi.org/10.1021/ja028458j.

(40) Finklea, H. O.; Hanshew, D. D. Electron-Transfer Kinetics in Organized Thiol Monolayers with Attached Pentaammine(Pyridine)Ruthenium Redox Centers. *J. Am. Chem. Soc.* **1992**, *114* (9), 3173–3181. https://doi.org/10.1021/ja000035a001.

(41) Ravenscroft, M. S.; Finklea, H. O. Kinetics of Electron Transfer to Attached Redox Centers on Gold Electrodes in Nonaqueous Electrolytes. *J. Phys. Chem.* **1994**, *98* (14), 3843–3850. https://doi.org/10.1021/j100065a047.

(42) Rowe, G. K.; Carter, M. T.; Richardson, J. N.; Murray, R. W. Consequences of Kinetic Dispersion on the Electrochemistry of an Adsorbed Redox-Active Monolayer. *Langmuir* **1995**, *11* (5), 1797–1806. https://doi.org/10.1021/la000052059.

(43) Hockett, L. A.; Creager, S. E. Redox Kinetics for Ferrocene Groups Immobilized in Impermeable and Permeable Self-Assembled Monolayers. *Langmuir* **1995**, *11* (6), 2318–2321. https://doi.org/10.1021/la00006a077.

(44) Carter, M. T.; Rowe, G. K.; Richardson, J. N.; Tender, L. M.; Terrill, R. H.; Murray, R. W. Distance Dependence of the Low-Temperature Electron Transfer Kinetics of (Ferrocenylcarboxy)-Terminated Alkanethiol Monolayers. *J. Am. Chem. Soc.* **1995**, *117* (10), 2896–2899. https://doi.org/10.1021/ja00115a022.

(45) Marcus, R. A. On the Theory of Electron-Transfer Reactions. VI. Unified Treatment for Homogeneous and Electrode Reactions. *J. Chem. Phys.* **1965**, *43* (2), 679–701. https://doi.org/10.1063/1.1696792.

(46) Weaver, M. J. Activation Parameters for Simple Electrode Reactions. Application to the Elucidation of Ion-Solvent Interactions in the Transition State for Heterogeneous Electron Transfer. *J. Phys. Chem.* **1979**, *83* (13), 1748–1757. https://doi.org/10.1021/j100476a013.

(47) Weber, K. S.; Creager, S. E. Reorganization Energetics for Ferrocene Oxidation/Reduction in Self-Assembled Monolayers on Gold. *J. Electroanal. Chem.* **1998**, *458* (1), 17–22. https://doi.org/https://doi.org/10.1016/S0022-0728(98)00303-9.

(48) Forster, R. J.; Loughman, P.; Keyes, T. E. Effect of Electrode Density of States on the Heterogeneous Electron-Transfer Dynamics of Osmium-Containing Monolayers. *J. Am. Chem. Soc.* **2000**, *122* (48), 11948–11955. https://doi.org/10.1021/ja002616u.

(49) Feldberg, S. W.; Sutin, N. Distance Dependence of Heterogeneous Electron Transfer through the Nonadiabatic and Adiabatic Regimes. *Chem. Phys.* **2006**, *324* (1), 216–225. https://doi.org/https://doi.org/10.1016/j.chemphys.2005.12.016.

(50) Magriñá, I.; Ortiz, M.; Simonova, A.; Hocek, M.; O' Sullivan, C. K.; Forster, R. J. Ferrocene-Containing DNA Monolayers: Influence of Electrostatics on the Electron Transfer Dynamics. *Langmuir* **2021**, *37* (11), 3359–3369. https://doi.org/10.1021/acs.langmuir.0c03485.

(51) Arinaga, K.; Fujita, S.; Abstreiter, G.; Tornow, M.; Rant, U.; Yokoyama, N. Dynamic Electrical Switching of DNA Layers on a Metal Surface. *Nano Lett.* **2004**, *4* (12), 2441–2445. https://doi.org/10.1021/nl0484494.

(52) Trewby, W.; Tavakol, M.; Jaques, Y. M.; Voïtchovsky, K. Towards Local Tracking of Solvated Metal Ions at Solid-Liquid Interfaces. *Mater. Today Phys.* **2024**, *44*, 101441. https://doi.org/https://doi.org/10.1016/j.mtphys.2024.101441.

(53) Israelachvili, J. *Intermolecular and Surface Forces*, 3rd ed.; Elsevier: Boston, 2011. https://doi.org/10.1016/C2009-0-21560-1.

(54) Lee, S. S.; Fenter, P.; Nagy, K. L.; Sturchio, N. C. Real-Time Observation of Cation Exchange Kinetics and Dynamics at the Muscovite-Water Interface. *Nat. Commun.* **2017**, *8* (1), 15826. https://doi.org/10.1038/ncomms15826.

(55) Paul, A.; Borrelli, R.; Bouyanfif, H.; Gottis, S.; Sauvage, F. Tunable Redox Potential, Optical Properties, and Enhanced Stability of Modified Ferrocene-Based Complexes. *ACS Omega* **2019**, *4* (12), 14780–14789. https://doi.org/10.1021/acsomega.9b01341.

(56) Bangle, R. E.; Schneider, J.; Conroy, D. T.; Aramburu-Trošelj, B. M.; Meyer, G. J. Kinetic Evidence That the Solvent Barrier for Electron Transfer Is Absent in the Electric Double Layer. *J. Am. Chem. Soc.* **2020**, *142* (35), 14940–14946. https://doi.org/10.1021/jacs.0c05226.

(57) Fumagalli, L.; Esfandiar, A.; Fabregas, R.; Hu, S.; Ares, P.; Janardanan, A.; Yang, Q.; Radha, B.; Taniguchi, T.; Watanabe, K.; Gomila, G.; Novoselov, K. S.; Geim, A. K. Anomalously Low Dielectric Constant of Confined Water. *Science (80-.).* **2018**, *360* (6395), 1339–1342. https://doi.org/10.1126/science.aat4191.

(58) Matyushov, D. V. Dynamical Effects in Protein Electrochemistry. *J. Phys. Chem. B* **2019**, *123* (34), 7290–7301. https://doi.org/10.1021/acs.jpcb.9b04516.

(59) Zitare, U. A.; Szuster, J.; Santalla, M. C.; Morgada, M. N.; Vila, A. J.; Murgida, D. H. Dynamical Effects in Metalloprotein Heterogeneous Electron Transfer. *Electrochim. Acta* **2020**, *342*, 136095. https://doi.org/https://doi.org/10.1016/j.electacta.2020.136095.

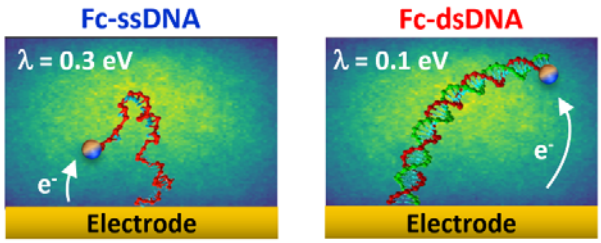

Low Solvent Reorganization Energy
High Thermal Activation Energy